In-Plane and Interfacial Thermal Conduction of Two-Dimensional Transition-Metal Dichalcogenides

Yifei Yu, Tamzid Minhaj, Lujun Huang, Yiling Yu, and Linyou Cao

Phys. Rev. Applied **13**, 034059 — Published 24 March 2020

DOI: 10.1103/PhysRevApplied.13.034059

In-Plane and Interfacial Thermal Conduction of Two-Dimensional Semiconductors

Yifei Yu[1§], Tamzid Minhaj[1§], Lujun Huang[1], Yiling Yu[1], Linyou Cao[1,2,3]*

[1]Department of Materials Science and Engineering, North Carolina State University, Raleigh NC 27695; [2]Department of Physics, North Carolina State University, Raleigh NC 27695; [3]Department of Electrical and Computer Engineering, North Carolina State University, Raleigh NC 27695.

§ contributed equally.

Abstract: We elucidate the dependence of the in-plane and interfacial thermal conduction of two-dimensional (2D) transition metal dichalcogenide (TMDC) materials (including MoS_2, WS_2, and WSe_2) on the materials' physical features, such as size, layer number, composition, and substrates. The in-plane thermal conductivity k is measured at suspended 2D TMDC materials and the interfacial thermal conductance g measured at the materials supported onto substrates, both with Raman thermometry techniques. The thermal conductivity k increases with the radius R of the suspended area following a logarithmic scaling as $k \sim \log(R)$. k also shows a substantial decrease from monolayer to bilayer, but only changes mildly with further increase in the layer number. In contrast, the interfacial thermal conductance g bears negligible dependence on the layer number. But g increases with the strength of the interaction between 2D TMDC materials and the substrate, substantially varying among different substrates. The result is consistent with theoretical predictions and clarifies much inconsistence in references. This work provides useful guidance for the thermal management in 2D TMDC materials and devices.

* To whom correspondence should be addressed.

Email: linyoucao@gmail.com

I. INTRODUCTION

Two-dimensional (2D) transition metal dichalcogenide (TMDC) materials such as MoS_2, WS_2, $MoSe_2$, and WSe_2 show remarkable electrical [1] and optical properties [2], and bear great promise for the development of novel devices in a wide range of fields, including integrated circuitry [3], optoelectronics [4], spintronics [5], piezoelectricity [6], and thermoelectricity [7]. One important issue for the device development is to manage the thermal dissipation in 2D TMDC materials, which is expected to be a major bottleneck for the device performance due to the atomically thin dimension of the materials. However, the fundamental understanding for the thermal conduction in 2D TMDC materials has remained relatively limited[8], which has limited the development of strategies for effective thermal management. For instance, whereas there are numerous studies on the in-plane thermal conductivity of 2D TMDC materials, the results show substantial inconsistence. The in-plane thermal conductivity of MoS_2 reported in references varies by one order of magnitude in the range of 13-120 W/m.K [9-12], and there is no clear clue about the cause of the inconsistence other than speculating difference in the quality of the materials studied or in the measurement techniques. Additionally, the correlation between the thermal conduction and physical features of 2D TMDC materials, such as size, composition, and layer number, is elusive. Knowledge of the correlation would provide useful guidance for the thermal management in 2D TMDC materials and devices.

Here we elucidate the dependence of the in-plane thermal conductivity and interfacial thermal conductance of 2D TMDC materials on the materials' physical features with Raman thermometry. We demonstrate that the in-plane thermal conductivity k increases with the size R of the materials following a logarithmic scaling as $k \sim \log(R)$, and also elucidate the dependence of k on the layer number and composition. Additionally, we show that the interfacial thermal

conductance *g* bears negligible dependence on the layer number but increases with the strength of the interaction between 2D TMDC materials and substrates. Our results are consistent with the prediction of many theoretical studies, and clarify much inconsistence in previous studies.

II. Experimental section

Synthesis and transfer TMDC flakes: All the TMDC flakes were obtained from 2Dlayer, which are made using chemical vapor deposition (CVD) reported in references.[13] The transfer of the TMDC flaks followed a surface-energy-assisted transfer approach that we have developed previously.[14] In a typical transfer process, 9 g of polystyrene (PS) with a molecular weight of 280000 g/mol was dissolved in 100 mL of toluene, and then the PS solution was spin-coated (3000 rpm for 60 s) on the as-grown substrate(SiO_2/Si). This was followed by a baking at 80−90 °C for 1 hour. A water droplet was then dropped at the edge of the original substrate. Due to the different surface energies of the TMDC flakes and the substrate, water molecules could penetrate the interface, resulting the delamination of the PS-monolayer assembly. We could pick up the polymer/TMDC flakes with a tweezers and transferred it to the quartz substrate with pre-patterned holes. After that, we baked the transferred PS-monolayer assembly at 130 °C for 15min. Finally, PS was removed by gently rinsing with toluene several times.

Raman Characterizations: Horiba Labram HR800 system with the excitation wavelength of 442 nm or 532 nm was used to measure the Raman spectra of 2D TMDC materials. The temperature dependent Raman measurement was carried out with the materials placed in Linkam heating Stage (THMS600) with controlled temperature, and the incidence used for the measurement is a focused 532nm laser with a power of no more than 90 mW, at which the laser-induced temperature increase is usually no more than 20^{o}C . All the power-dependent Raman measurement for the suspended

samples were performed at room temperature using a focused 442 nm laser in radius of 0.66 μm, and those for the supported samples using a focused 532 nm laser in radius of 0.52 μm.

III. RESULTS AND DISCUSSION

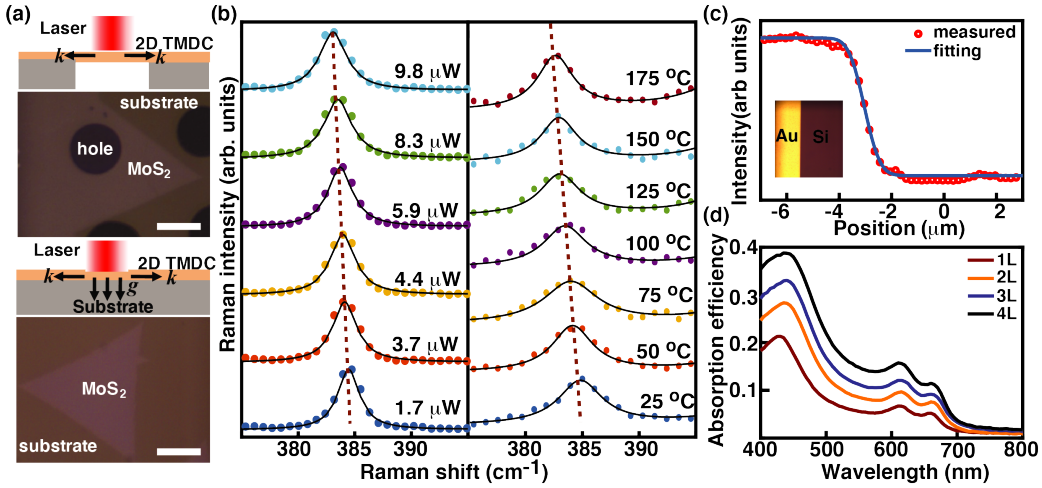

FIG.1. Raman thermometry measurement for the in-plane and interfacial thermal conduction of 2D TMDC materials. (a) Configuration for the Raman thermometry measurement of in-plane thermal conductivity k and interfacial thermal conductance g at suspended (top) and supported (bottom) 2D TMDC materials, and typical optical images for suspended and supported MoS_2 flakes. The scale bar is 10 μm. (b) Dependence of Raman shift of the E^1_{2g} peak of suspended monolayer MoS_2 as a function of absorbed laser power (left) and temperature (right). The power-dependent Raman spectra were collected using a focused 442 nm laser in radius of 0.66 μm at room temperature. The temperature-dependent Raman were collected using a 532 nm with a power of 90 μW, which is expected to generate temperature increase no more than 20 °C. The dashed lines serve as a vision guide. (c) Measured and fitted spatial distribution of the Raman intensity across a sharp edge of a gold pad deposited on Si substrates, which is shown in the inset. (d) Calculated spectral absorption efficiency of suspended MoS_2 flakes with different layer numbers.

We started with studying single crystalline MoS_2 flakes grown using a CVD process reported previously. [13] We measured the in-plane thermal conductivity and interfacial thermal conductance of the flakes with a well-established Raman thermometry. [15,16] The interfacial thermal conductance (ITC) was measured at the MoS_2 flakes supported on substrates, while the

in-plane thermal conductivity was measured at suspended flakes that were prepared by transferring the MoS_2 flakes from growth substrates (either sapphire or Si/SiO_2) onto quartz substrate pre-patterned with micrometer-scale holes.[14] The use of quartz substrates is to minimize interference of the incident light with the light reflected back from the bottom of the hole, which would otherwise cause substantial error in the evaluation of the absorption efficiency. Fig. 1(a) shows a schematic illustration for the measurement configuration and typical optical images of the substrate-supported and suspended MoS_2 flakes. The Raman thermometry involves the measurement of a power shift rate (PSR), *i.e.* dependence of the Raman frequency shift on absorbed incident laser power, and a Raman temperature coefficient (TC), *i.e.* dependence of the Raman frequency shift on temperature (Fig. 1(b)). As the atomically thin materials are very vulnerable, we ensured no material degradation during the measurement for every flake studied by confirming the Raman spectra collected before and after the thermometry measurement are similar. The accuracy of Raman thermometry hinges on precise information about the size w of the focused incident laser beam and the absorption efficiency α of the flakes for the incident laser [17]. We find out the value of w by mapping Raman intensity across the sharp edge of a gold pad deposited on silicon substrates (Fig. 1(c)). We also calculate the absorption efficiency α using the refractive index of 2D MoS_2 reported previously[18] as shown in Fig. 1(d). We have confirmed that the optical response of 2D MoS_2 calculated using the refractive index matches the result of experimental measurement reasonably well (Fig. S1). [19] The calculated absorption efficiency is also consistent with what was reported in references [20].

We extract the in-plane thermal conductivity k and interfacial thermal conductance g by fitting the experimental results to an analytic model derived from the Fourier equation of heat conduction. Briefly, we consider the thermal conduction in the flakes to be diffusive. As a result,

the thermal conduction of the suspended flakes under the incidence of a focused Gaussian laser beam is governed by the following differential equations in a cylindrical coordinate as [15]

$$kt\frac{1}{r}\frac{\partial}{\partial r}\left(r\frac{\partial T}{\partial r}\right)+\frac{\alpha Q}{\pi w^2}exp\left(-\frac{r^2}{w^2}\right)=0 \qquad (r\le R) \qquad (1)$$

$$kt\frac{1}{r}\frac{\partial}{\partial r}\left(r\frac{\partial T}{\partial r}\right)-g(T-T_0)=0 \qquad (r>R) \qquad (2)$$

where T_0 is the ambient temperature, Q is the incident power, R is the radius of the suspended area, and t is the thickness of the flakes. We also have the differential equation governing the heat dissipation of the supported flakes under the incidence of a focused Gaussian laser beam as

$$kt\frac{1}{r}\frac{\partial}{\partial r}\left(r\frac{\partial T}{\partial r}\right)-g(T-T_0)+\frac{\alpha Q}{\pi w^2}exp\left(-\frac{r^2}{w^2}\right)=0 \qquad (3)$$

By applying appropriate boundary conditions, we can find out the temperature of the suspended flakes to be

$$T(r)=\frac{\alpha Q\left[1-exp\left(-\frac{r^2}{w^2}\right)\right]}{2\pi kR\sqrt{b}t}\frac{K_0(\sqrt{b}r)}{K_1(\sqrt{b}R)}+T_0 \qquad (r\ge R) \qquad (4)$$

$$T(r)=T_1+\frac{\alpha Q}{2\pi kt}\ln\left(\frac{R}{r}\right)+\frac{\alpha Q}{4\pi kt}\left[Ei\left(-\frac{r^2}{w^2}\right)-Ei\left(-\frac{R^2}{w^2}\right)\right] \qquad (r\le R) \qquad (5)$$

where $b = g/(k.t)$ and T_1 is the temperature at $r = R$ that may be obtained by substituting $r = R$ into eq.(4). I_0, K_0, and Ei are the zeroth-order modified Bessel function of the first kind, the modified Bessel function of the second kind, and exponential integral functions, respectively. By the same token, we can find the temperature of the supported flakes as

$$T(r)=\frac{\alpha Q}{kt\pi w^2}\int_0^\infty M(k,g,r,y)exp\left(-\frac{y^2}{w^2}\right)ydy+T_0 \qquad (6)$$

$$M(k,g,r,y)=K_0(\sqrt{b}r)I_0(\sqrt{b}y) \qquad (y\le r) \qquad (7)$$

$$M(k,g,r,y)=I_0(\sqrt{b}r)K_0(\sqrt{b}y) \qquad (r\le y) \qquad (8)$$

It is worthwhile to point out that some previous studies on Raman thermometry use an incorrect equation for the laser-induced temperature distribution of substrate-supported 2D materials due to the application of wrong boundary conditions[15]. The in-plane thermal conductivity *k* and the interfacial thermal conductance *g* can be found out by fitting the Raman measurement result to the model. More specifically, we experimentally find out the temperature of the flakes under the incidence of a focused Gaussian laser using Raman spectroscopy. Then we can extract out the value of *k* and *g* by fitting the temperature obtained from Raman measurement with a Gaussian-weighted temperature as

$$T_m = \frac{\int_0^\infty T(r) exp\left(-\frac{r^2}{w^2}\right) r dr}{\int_0^\infty exp\left(-\frac{r^2}{w^2}\right) r dr} \qquad (9)$$

This analytical model involves some assumptions and approximations, but we find all of them are reasonable in our experiment. First, it assumes that the temperature of the substrate does not change during the Raman measurement. For our suspended flakes, the radius of the focused laser beam (for instance, the radius of the focused 442 nm laser is 0.66 μm) is much smaller than the size of the suspended area, and we have confirmed that the majority of the laser-induced temperature increase is confined in the suspended area as illustrated in Fig. S2. In experiment we obtained similar thermal conductivity at the MoS_2 flakes suspended on the holes in either quartz or gold substrates. This indicates that the thermal conduction in the substrate has negligible influence in the heat dissipation of the suspended flakes, confirming very mild temperature increase at the substrate. For the supported flakes, we monitored the Raman spectra of the substrate during the measurement and confirmed that the temperature increase at the substrates studied is negligible compared to the temperature increase in the flakes (Fig. S3). Second, the model ignores the heat dissipation through other pathways than thermal conduction, including thermal radiation

and thermal convection. In our system, the thermal power dissipated by thermal radiation is estimated to be no more than 0.11 W/cm^2, which is more than four orders of magnitude lower than the absorbed incident power. We also found no difference in the laser-induced temperature increase at the suspended flakes under both ambient pressure and vacuum (< 0.01 Torr) (Fig. S4). This indicates a negligible contribution of thermal convection, which strongly depends on the pressure, to the heat dissipation. Additionally, the model does not consider the variation of the absorption efficiency α with temperature. This is reasonable as because the temperature increase in our experiment is not huge (usually < 120^{o}C), and the change in the absorption efficiency is expected no more than 10%. [21]

We measured the thermal conductivity at the monolayer MoS_2 flakes suspended on holes with different sizes. Fig. 2(a) - (b) shows typical PSR and TC measured at the suspended MoS_2 flakes, and the thermal conductivity derived from the measurement results are plotted in Fig. 2©. Tabulated measurement results and related thermal conductivities for the suspended MoS_2 flakes are provided in Table S1 of Supplementary Information. MoS_2 have two major characteristic Raman peaks, E^1_{2g} (~ 385 cm^{-1}) and A_{1g} (~ 405 cm^{-1}). We have confirmed that the measurement for either peak of the suspended flakes usually give rise to similar thermal conductivity (Fig.S5). However, the measurement on E^1_{2g} is generally more credible, because the A_{1g} peak is susceptible to the effect of doping and could be affected by the doping effects of impurities or adsorbents. Therefore, we focus on the E^1_{2g} peak in this work. Significantly, the thermal conductivity monotonically increases with the suspended size. The size dependence of the thermal conductivity may be reasonably fitted with a logarithmic scaling as $k \sim log(R)$. Our result is consistent with theoretical prediction. Numerous theoretical studies have predicted that the thermal conductivity of two dimensional Fermi-Pasta-Ulam (FPU) rectangle and disk lattices diverges with size

following a logarithmic scaling. [22-26] In particular, recent studies explicitly predicted a logarithmic size scaling in the thermal conductivity of 2D TMDC materials [27] [28]. Our result is also consistent with the measurement for suspended graphene ribbons, which shows a logarithmic size scaling in thermal conductivity [29,30]. The logarithmic scaling is due to the anharmonicity of phonon potential and boundary scattering in 2D materials. While the phonon mean free path of 2D TMDC materials is reported to be tens of nanometers [31], orders of magnitude smaller than the suspended size in our work, the value just represents an average of effective mean free path of a broad spectra of phonons with different frequency and polarizations. According to theoretical calculation[31], low-frequency phonons, which have long mean free path, may play a significant role in the thermal conductivity of 2D materials. More low-frequency thermal phonons may be excited with the sample size increasing, leading to increase in the thermal conductivity.

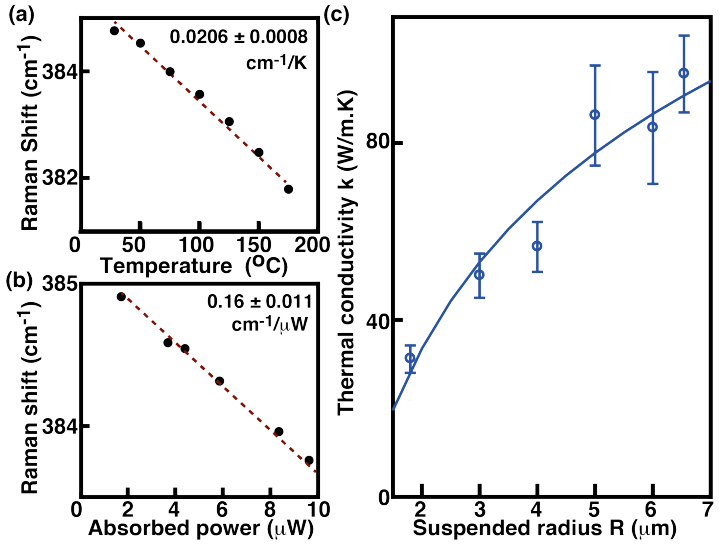

FIG.2. Size dependent thermal conductivity of monolayer MoS_2. Typical shift of E^1_{2g} Raman peak as a function of (a) temperature and (b) adsorbed incident laser power. The dots are the experimental measurement, and the dashed line is a fitting for the experimental result. (c) Thermal conductivity of monolayer MoS_2 as a function of the suspended size. The solid line is the logarithmic fitting for the mean value of the measurement.

We also measured the thermal conductivity of suspended MoS_2 flakes with different layer numbers. The layer number of the flakes are identified by a combination of optical contrast and Raman measurement as illustrated in the insets of Fig. 3(a)-(b). Similar to the measurement for the monolayer, the power-dependent Raman spectra for the multilayer MoS_2 were collected at room temperature using a 442 nm laser in a radius of 0.66 μm at room temperature, and the temperature-dependent Raman were collected using a 532 nm laser with a power expected to generate temperature increase no more than 20 ºC. We obtain the thermal conductivity by fitting the measurement result with eq. (9). Fig. 3(a) shows the thermal conductivity of bilayer MoS_2 flakes as a function of the suspended size (red dots). Similar to the monolayer counterpart, the bilayer's thermal conductivity increases with the suspended size, and the size dependence may be reasonably fitted as $k \sim \log(R)$. While it is difficult to prepare enough number of suspended tri-layers and quadra-layers for systematic studies, the result we obtained from a limited number of tri-layer and quadra-layer samples implies a logarithmic size scaling as well (see Table S1 for the PSR and TC measurement results of fewlayer MoS_2). The measurement at the flakes with different layer numbers also allow us to elucidate the dependence of the thermal conductivity on the layer number. To illustrate this notion, we compare the thermal conductivity of suspended MoS_2 flakes with different layer numbers but the same size (4 μm, without losing generality) as shown in Fig. 3b. The thermal conductivity substantially decreases from monolayer to bilayer, but shows very mild change for further increase in the layer number. This layer dependence is similar to what was observed at graphene [32], and also consistent with previous theoretical studies that predict a decrease in the thermal conductivity of 2D TMDC materials with increase of the layer number [33].

We can get more insight into the size and layer dependence of the thermal conductivity by comparing our result with that of bulk MoS_2. Previous studies have reported that the in-plane thermal conductivity of bulk MoS_2 varies between 85-110 W/m.K depending on the size of the incident laser beam. This dependence on the laser beam size corroborates the size dependence we observed at 2D MoS_2. Both increase of the laser spot and the material size enable the involvement of thermal phonons with longer mean free path. Additionally, the thermal conductivity of bulk MoS_2 is similar to that of large suspended monolayer MoS_2. This indicates that MoS_2 actually have similar thermal conductivity regardless the layer number, as far as the size is large enough. We believe that the observed layer dependence of the thermal conductivity is due to difference in the phonon properties[34] as well as the limited size of the suspended MoS_2 flakes. The contribution of the thermal phonons with long mean free path (MFP) to thermal conduction could be larger in fewlayer MoS_2 than in monolayer MoS_2, and the micrometer-scale size of the fewlayer flakes might only enable the involvement of part of the long-MFP phonons. We expect the thermal conductivity of fewlayer MoS_2 would show thermal conductivity comparable to that of bulk MoS_2 if the size could be substantially increased.

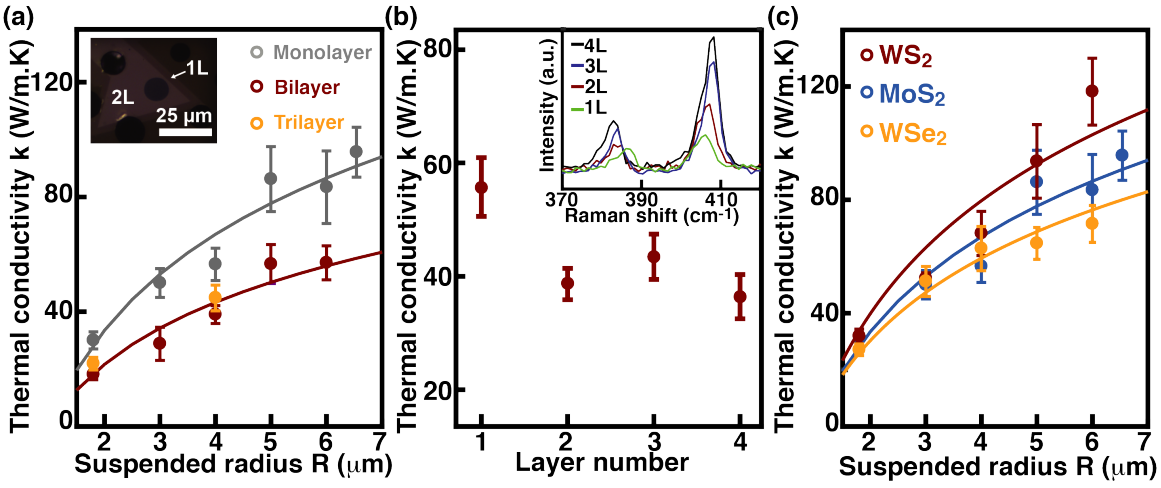

FIG.3. Layer and composition dependence of the thermal conductivity in 2D TMDC materials. (a) Thermal conductivity of bilayer MoS_2 as a function of the suspended size (red color). The solid line is the logarithmic fitting $k \sim log(R)$. The results in gray color is the size-dependent thermal conductivity of monolayer MoS_2. Also plotted are the results collected from trilayer MoS_2 flakes (orange color). Inset: a typical optical image of suspended bilayer MoS_2 flakes, in which the bilayer can be found showing distinct optical contrast from monolayers. (b) Thermal conductivity of MoS_2 flakes as a function of the layer number. All the results collected from the flakes suspended on holes in radius of 4 μm. The inset is the Raman spectroscopy collected from these flakes with different layer numbers. (c) Thermal conductivity of monolayer WS_2 (red color) and WSe_2 (orange color) as a function of the suspended size. Also plotted in the thermal conductivity of MoS_2 (blue color). The solid lines are the associated logarithmic fitting $k \sim log(R)$.

The logarithmic size dependence of thermal conductivity holds for other 2D TMDC materials such as WS_2 and WSe_2. Fig. 3(c) shows the thermal conductivity measured from suspended single-crystalline monolayer WS_2 and WSe_2 flakes that were grown and transferred in ways similar to the suspended MoS_2 flakes. The experimental conditions for the PSR and TC measurements of WS_2 and WSe_2 are also similar to those used for the measurement of monolayer MoS_2. Again, the thermal conductivity of monolayer WS_2 and WSe_2 increases with the suspended size, and the size dependence can be reasonably fitted with a logarithmic scaling as $k \sim \log(R)$. This is understandable because the logarithmic scaling is rooted in the two-dimensionality of the lattice regardless the specific composition. [22-26] For the TMDC materials measured, WS_2 has the highest thermal conductivity, followed by MoS_2 and WSe_2. The higher thermal conductivity of WS_2 than that of MoS_2 is surprising. Generally, phonon thermal conductivity is related with four parameters: atomic mass, interatomic bonding, crystal structures, and phonon anharmonicity[35]. All these TMDC materials have similar crystal structure with negligible difference in phonon anharmonicity and atomic bonding. For instance, the difference of phonon anharmonicity (Gruneisen parameter) and atomic bonding between MoS_2 and WS_2 is around 6% and 4%, respectively [35]. However, W atom is 40% heavier than Mo atom, and WS_2 is intuitively expected to have lower thermal conductivity than MoS_2 since heavier atoms tend to give rise to

lower thermal conductivity. Our observed higher thermal conductivity at WS_2 is consistent with a recent theoretical study also predicts a higher thermal conductivity in WS_2 than MoS_2. [27] The theoretical study ascribes it to a lager phonon frequency gap between the acoustic and optical phonon branches in WS_2, which may result in less phonon-phonon scattering [27].

Besides from the in-plane thermal conductivity, we studied the interfacial thermal conductance (ITC) of 2D TMDC materials and obtained much new fundamental understanding as well. We use single-crystalline MoS_2 flakes with different layer numbers on sapphire substrates as an example to illustrate the main discovery. Similar to the suspended flakes, the layer number of the substrate-supported flakes can be identified from optical contrast and Raman measurement (Fig. 4(a) and 4(b)). We performed Raman thermometry measurement at as-grown MoS_2 flakes on sapphire substrates (Fig. 4(c)-(d)). The TC measurement condition is similar to those used for the suspended flakes, but the PSR measurement of the supported flakes was conducted using a focused 532 nm laser with a radius of 0.52 μm at room temperature. The ITC derived from fitting the measurement result with eq.(9) is plotted in Fig. 4(e) (orange dots). Unlike the layer dependence of the in-plane thermal conductivity, the ITC of MoS_2 shows negligible dependence on the layer number, maintaining to be around 16-17 $MW/m^2.K$ regardless the layer number (Fig. 4(e)). Note that we assume all the layers of fewlayer MoS_2 are under thermal equilibrium (having the same temperature) in the derivation of the ITC from experimental measurement using eqs. (6)-(9). This assumption is reasonable because the interlayer thermal conductance is much larger than the interfacial one between the MoS_2 and underlying substrates. Previous studies have demonstrated that the interlayer thermal conductivity is 2.0 ± 0.3 $W.m^{-1} K^{-1}$,[36] and this corresponds to a interlayer thermal conductance 6.33 $GW.m^{-2} K^{-1}$ as the interlayer distance is 0.31nm, which is more than two orders of magnitude larger than the interfacial thermal conductance. While we focus on MoS_2, the layer

independence of the ITC holds true for other 2D materials. For instance, we measured the ITC of single crystalline WS_2 flakes grown on sapphire substrates. It is obviously larger (~ 30 MW/m^2.K) than that of the MoS_2 flakers, but shows a similar layer independence on the layer number (Fig. 4(d) red dots). Additionally, previous studies also reported the ITC of graphene independent of the layer number [37]. It is well accepted that the interfacial thermal conduction of dielectric materials is carried out by the interfacial transfer of phonons and governed by two factors, matching of the phonon spectra of the objects involved and strength of the interfacial bonding. [38-40] The observed layer independence of the ITC implies no layer dependence in the phonon spectra matching and interaction between substrates and the MoS_2 .

Our experimental result indicates that the ITC of 2D TMDC materials strongly depends on the strength of the interaction between the materials and the substrates. We measured the ITC of the MoS_2 flakes transferred from growth substrates (sapphire) onto another sapphire substrate. The transfer follows a surface energy assisted transfer process we developed previously, and we have confirmed no degradation in the quality of the flakes during the transfer process [14]. The ITC of the transferred flakes shows no dependence on the layer number as well (blue dots in Fig. 4€), but is 40-50% lower than the as-grown counterparts, being in the range of 8-10 MW/m^2.K,. This is because the transferred flakes interact with the substrates less intimately than the as-grown counterparts. We also measured the ITC of monolayer MoS_2 flakes transferred onto other substrates. The ITC substantially varies with the substrates, for instance, GaN (6.1 ± 1.0 MW/m^2.K), Au (8.0 ± 1.2 MW/m^2.K), Cu (7.1 ± 1.1 MW/m^2.K), Ni (2.3 ± 0.5 MW/m^2.K), and HOPG (13 ± 2.0 MW/m^2.K). A detailed discussion for the mechanism underlying the substrate-dependent variation is beyond the scope of this work. However, we believe that the interaction strength of MoS_2 with the substrates plays an important role in the observed substrate-dependent

variation. For instance, 2D materials substrates like HOPG may enable higher ITC than conventional 3D substrates because 2D TMDC materials interact with 2D substrate stronger than with 3D substrates. Au and Cu may enable higher ITC than many other metals because Au and Cu have a tendency to form covalent bonding with sulfur atoms even at ambient environment [41].

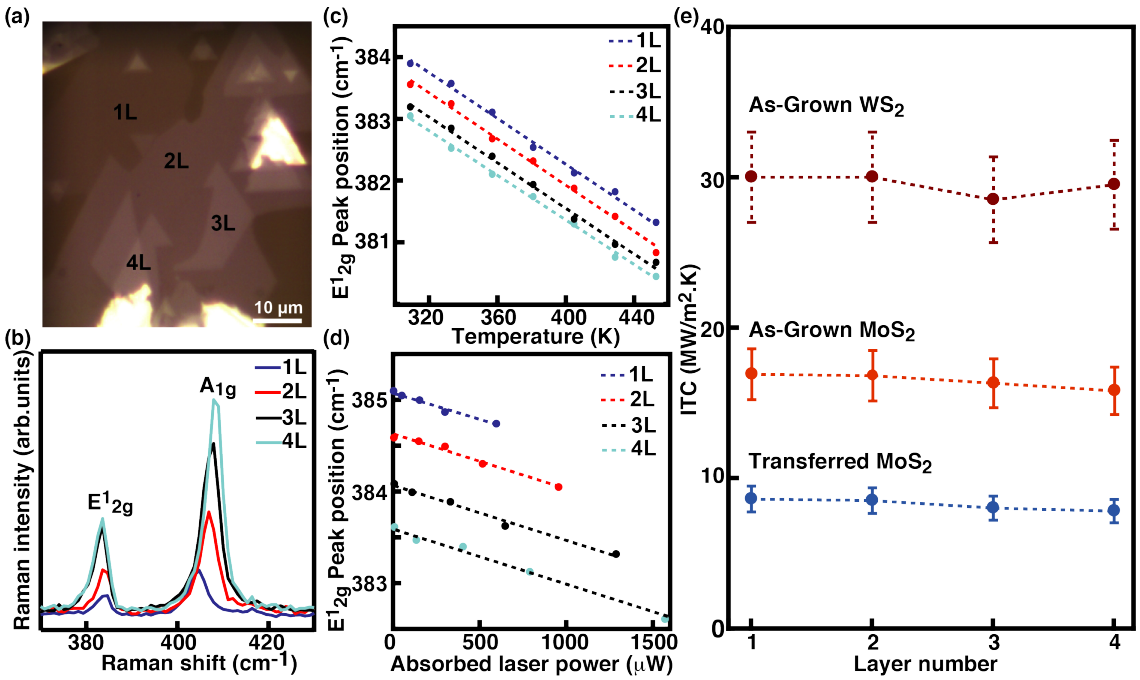

FIG. 4. Layer-independent interfacial thermal conductance of MoS_2. (a) Optical images of single-crystalline MoS_2 flakes with different layer numbers on sapphire substrates, in which the layer numbers are labelled as shown. (b) Raman spectra of the flakes with different layer numbers. Raman shift of the E^1_{2g} peak of the MoS_2 flakers as a function of (c) temperature and (d)absorbed laser power. The dots are experimental results and the dashed lines are fitting. The TC measurement condition is similar to those used for the suspended flakes. The PSR measurement was conducted using a focused 532 nm laser with a radius of 0.52 μm at room temperature. (e) Measured ITC of as-grown MoS_2 flakes (orange) and WS_2 flakes (red) on sapphire substrates as a function of the layer number. Also plotted is the ITC of transferred MoS_2 flakes (blue) on sapphire substrates. The dots are experimental results and the dashed lines serve as vision guide.

From the stand point of device development, it is important to understand the ITC of 2D TMDC materials on silicon substrates with thermally grown silicon oxides, which are expected to be widely used in 2D TMDC material devices. We performed Raman thermometry measurements

at as-grown MoS_2 flakes on the SiO_2/Si substrates with different thickness in the SiO_2 layer, and use the above-mentioned analytical model to extract the ITC. The result is plotted in Fig. 5a. The ITC shows no dependence on the layer number (Fig. 5(a) inset), but monotonically decreases with increase in the thickness of the SiO_2 layer (Fig. 5(a)). The result shown in Fig. 5(a) actually represents the effective interfacial thermal conduction collectively contributed by multiple steps in the system. As illustrated in Fig. 5(b) inset, these steps include the interfacial thermal conduction between the 2D MoS_2 and SiO_2 ($G_{2D/SiO2}$), the thermal conduction in the SiO_2 layer (k_{SiO2}), the interfacial thermal conduction at the SiO_2/Si interface ($G_{SiO2/Si}$), and the thermal conduction in the Si (k_{Si}). We expect $G_{SiO2/Si}$ (> 600 MW/m^2.K) [42] and k_{Si} (130 W/m.K) [43] to be much larger than $G_{2D/SiO2}$ and k_{SiO2}, and this is supported by the negligible temperature increase at the Si substrate during the Raman thermometry measurement (Fig. S3). Therefore, the effective thermal conductance G_{eff} may be correlated to $G_{2D/SiO2}$ and k_{SiO2} as $1/G_{eff} = 1/G_{2D/SiO2} + d/k_{SiO2}$, where d is the thickness of the SiO_2 layer. The true interfacial thermal conductance $G_{2D/SiO2}$ can be found out from the measured effective ITC G_{eff}. We plot the reciprocal of the result in Fig. 5(a) ($1/G_{eff}$) as a function of the thickness of the SiO_2 layer in Fig. 5(b). A linear fitting of the result indicates that $G_{2D/SiO2}$ is 18.6 MW/m^2.K, and the thermal conductivity of thermally grown SiO_2 k_{SiO2} is around 1.377 W/m.K[44], both of which are reasonably consistent with what have been reported in references. [45-47]

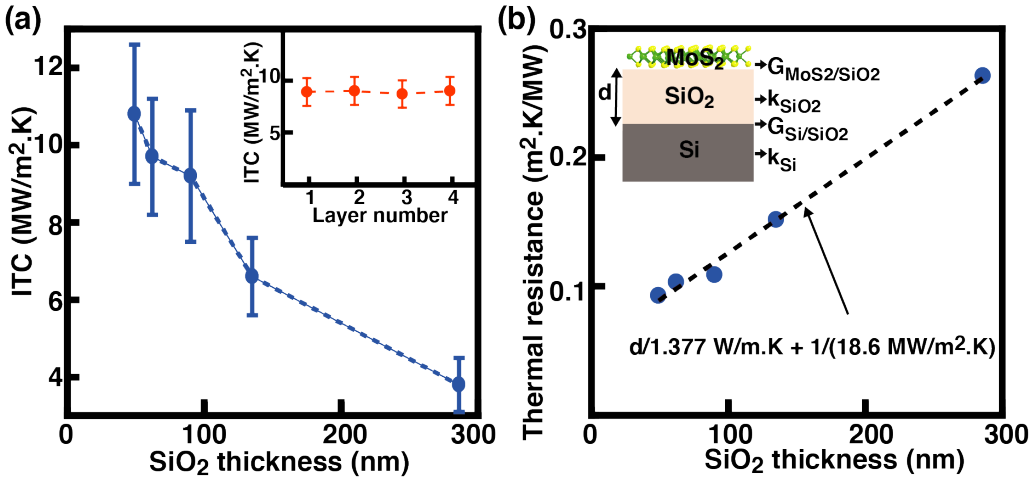

FIG. 5. Interfacial thermal conductance of monolayer MoS_2 on SiO_2/Si substrates with different SiO_2 thickness. (a)Measured effective ITC of MoS_2 on SiO_2/Si substrates as a function of the thickness of the SiO_2 layer. Inset: measured ITC of MoS_2 flakes with different layer number on SiO_2/Si substrates. The TC measurement condition is similar to those used for the suspended flakes. The PSR measurement was conducted using a focused 532 nm laser with a radius of 0.52 μm at room temperature. (b) The reciprocal of the effective ITC (thermal resistance) as a function of the thickness of the SiO_2 layer, in which the error bar is removed for vision convenience. The dashed line is a linear fitting. The inset schematically illustrates all the steps involved in the thermal dissipation of MoS_2 on SiO_2/Si substrates with 90 nm thermally grown SiO_2.

TABLE 1. Comparison for Thermal Conductivity measured at suspended MoS_2

Ref.	Method	Layer Number	Suspended Size (μm)	Thermal Conductivity (W/m-K)	Sample Type
This work	**Raman**	**1**	**Radius:1.8**	**32.5 ± 3.4**	**CVD**
Yan et al.[43]	Raman	1	Radius:0.6	34.5 ± 4	Exfoliated
Bae et al.[21]	Raman	1	Radius:1.8	36.6 (13.3±1.4)§	CVD
Yarali et al.[23]	Micro-bridge	1	Length:1.31 ± 0.06 Width:8.38 ± 0.89	30 ± 3.3	CVD
Yarali et al.[23]	Micro-bridge	1	Length:1.1 ± 0.063 Width:10.8 ± 0.63	35.5 ± 3	CVD
Zhang et al.[22]*	Raman	1	Radius:2.0	84 ± 17	Exfoliated
This work	**Raman**	**2**	**Radius:1.8**	**18.1 ± 1.8**	**CVD**
Zhang et al.[22]*	Raman	2	Radius:2.0	77 ± 25	Exfoliated
Bae et al.[21]	Raman	2	Radius:1.8	15.6 ± 1.5	CVD
This work	**Raman**	**4**	**Radius:4.0**	**36.9 ± 4.9**	**CVD**
Jo et al.[49]	Micro-bridge	4	Length: 3.0 Width: 5.2	44-50	Exfoliated
Aiyiti et al.[45]	Micro-bridge	4	Length: 2.0 Width: 3.0	34 ± 5	Exfoliated

Aiyiti et al.[45]	Micro-bridge	4	Length: 3.0 Width: 3.82	31 ± 4	Exfoliated
Aiyiti et al.[45]	Micro-bridge	5	Length:1.0 Width:5.87	30 ± 3	Exfoliated
Jo et al.[49]	Micro bridge	7	Length:8.0 Width:2.2	48-52	Exfoliated
Bae et al.[21]	Raman	(10-14)	Radius:1.8	43.4 ± 9.1	CVD

Notes: * These results are somehow different with ours. § The value in the parenthesis is the original value presented in the paper, and 36.6 is what we obtained using the correct absorption efficiency.

Our result clarifies much inconsistency in the thermal conduction properties of 2D materials reported in references. For instance, the in-plane thermal conductivity of 2D MoS_2 reported in references shows substantial variation. [10,36,48-52] We find that one major reason for the variation lies in the difference in sample size and layer number. To illustrate this notion, we summarize the previously reported thermal conductivities of MoS_2 along with our result in Table 1. The previous results include the thermal conductivities measured using either Raman thermometry or micro-bridge and at the materials prepared by either CVD processes or exfoliation. To ensure fair comparison, we only list the results in the references that provide enough experimental details (such absorption efficiency, suspended size, and layer number) allowing us to re-analyze the measurement result. As shown in Table 1, regardless the measurement techniques and the preparation method, most of the previous results are reasonably consistent with our results. The consistence of our results with the results obtained from micro-bridge measurement also supports the accuracy of our Raman thermometry measurement. Additionally, many previous studies reported the ITC of 2D materials on SiO_2/Si substrates [12,21,37,46], but little attention has been put on the effect of the thickness of SiO_2 layer on the measurement result.

Our result also provides useful guidance for the thermal management of 2D TMDC materials. It suggests that the interfacial thermal conduction would be dominant over the in-plane

thermal conduction for the heat dissipation of 2D TMDC materials. We use substrate-supported 2D material devices with a circular heating zone in radius of r as an example to illustrate this notion. The power dissipation by the interfacial (P_I) and lateral (P_L) thermal conduction may be written as $P_I = g\pi r^2\Delta T$ and $P_L = 2\pi rtkdT/dr$. For simplicity, we assume the temperature gradient in the lateral direction is linear and confined into the heating zone, *i.e.* $dT/dr = \Delta T/r$. Then P_L can be written as $P_L = 2\pi kt\Delta T$. For the interfacial thermal conduction to be more efficient in heat dissipation, we need to have $gr^2 \geq 2kt$, which gives rise to $r \geq (2kt/g)^{1/2}$. While we measured in-pane thermal conductivity at suspended 2D TMDC materials, the thermal conductivity of substrate-supported 2D TMDC materials is expected to be similar to that of suspended few layers. This is because the substrates affect could be similar to the effect of adding more layers [37,53,54] [55]. Without losing generality, we consider k = 20 W/m.k, and g = 2-20 MW/m^2.k and the critical value of $(2kt/g)^{1/2}$ is in the range of 30-100 nm. Any practical device would have heating area larger than this (even a single field effect transistor in integrated circuits could be in smaller size, the overall size of a practical integrated circuit would be much larger.). Therefore, engineering the interfacial thermal conduction should be the main strategy for the thermal management of 2D TMDC materials and devices. Our result also indicates using different layer number does not make any substantial difference in the interfacial thermal conduction, but engineering the substrates, such as the interaction strength with the materials and the thickness of the oxide layer in Si/SiO_2 substrates, provides an efficient strategy to control the heat dissipation of 2D TMDC materials.

IV. CONCLUSION

In conclusion, we have presented new fundamental understanding for the thermal conduction of 2D TMDC materials, including in-plane thermal conductivity and interfacial thermal conductance.

We elucidate the dependence of the thermal conduction on the physical features of the system, including size, layer number, composition, and substrates. Most importantly, we find that the in-plane thermal conductivity k increases with the radius R of the suspended area following a logarithmic scaling as $k \sim \log(R)$. k also shows some dependence on the layer number, substantially decreasing from monolayer to bilayer but only changing mildly with further increase in the layer number. In contrast, the interfacial thermal conductance g shows little dependence on the layer number. But g increases with the strength of the interaction between 2D TMDC materials and the substrate, substantially varying among different substrates. The Our results are consistent with the prediction of many theoretical studies, and clarify much inconsistence of the result in previous studies.

Acknowledgements
This work was supported by a CAREER award from the National Science Foundation (DMR-1352028), and partially by the grants of ECCS-1508856 and EFMA 1741693 from the National Science Foundation. The authors acknowledge Dr. Y. Zhu for providing access to a Horiba Labram HR800 system and C. Z. for assistance with the synthesis of WSe_2 flakes, and also acknowledge the use of the Analytical Instrumentation Facility (AIF) at North Carolina State University, which is supported by the State of North Carolina and the National Science Foundation.

References:

[1] A. Allain and A. Kis, Electron and hole mobilities in single-layer WSe2, ACS Nano **8**, 7180 (2014).
[2] M. Bernardi, C. Ataca, M. Palummo, and J. C. Grossman, Optical and electronic properties of two-dimensional layered materials, Nanophotonics **6**, 479 (2017).
[3] H. Wang, L. Yu, Y.-H. Lee, Y. Shi, A. Hsu, M. L. Chin, L.-J. Li, M. Dubey, J. Kong, and T. Palacios, Integrated circuits based on bilayer MoS2 transistors, Nano Lett. **12**, 4674 (2012).
[4] S. Salehi and A. Saffarzadeh, Optoelectronic properties of defective MoS2 and WS2 monolayers, J. Phys. Chem. Solids, **121**, 172 (2018).
[5] N. Zibouche, A. Kuc, J. Musfeldt, and T. Heine, Transition-metal dichalcogenides for spintronic applications, Ann. Phys-Berlin, **526**, 395 (2014).
[6] W. Wu, L. Wang, Y. Li, F. Zhang, L. Lin, S. Niu, D. Chenet, X. Zhang, Y. Hao, and T. F. Heinz, Piezoelectricity of single-atomic-layer MoS 2 for energy conversion and piezotronics, Nature **514**, 470 (2014).
[7] K. Hippalgaonkar, Y. Wang, Y. Ye, D. Y. Qiu, H. Zhu, Y. Wang, J. Moore, S. G. Louie, and X. Zhang, High thermoelectric power factor in two-dimensional crystals of Mo S2, Phys. Rev. B **95**, 115407 (2017).

[8] X. Gu and R. Yang, Phonon transport and thermal conductivity in two-dimensional materials, Annu. Rev. Heat Transfer **19** (2016).
[9] J. J. Bae, H. Y. Jeong, G. H. Han, J. Kim, H. Kim, M. S. Kim, B. H. Moon, S. C. Lim, and Y. H. Lee, Thickness-dependent in-plane thermal conductivity of suspended MoS2 grown by chemical vapor deposition, Nanoscale **9**, 2541 (2017).
[10] R. Yan, J. R. Simpson, S. Bertolazzi, J. Brivio, M. Watson, X. Wu, A. Kis, T. Luo, A. R. Hight Walker, and H. G. Xing, Thermal conductivity of monolayer molybdenum disulfide obtained from temperature-dependent Raman spectroscopy, ACS Nano **8**, 986 (2014).
[11] M. Yarali, X. Wu, T. Gupta, D. Ghoshal, L. Xie, Z. Zhu, H. Brahmi, J. Bao, S. Chen, and T. Luo, Effects of Defects on the Temperature-Dependent Thermal Conductivity of Suspended Monolayer Molybdenum Disulfide Grown by Chemical Vapor Deposition, Adv. Func.Mater. **27**, 1704357 (2017).
[12] X. Zhang, D. Sun, Y. Li, G.-H. Lee, X. Cui, D. Chenet, Y. You, T. F. Heinz, and J. C. Hone, Measurement of lateral and interfacial thermal conductivity of single-and bilayer MoS2 and MoSe2 using refined optothermal Raman technique, ACS Appl. Mater. Interfaces **7**, 25923 (2015).
[13] Y. H. Lee, X. Q. Zhang, W. Zhang, M. T. Chang, C. T. Lin, K. D. Chang, Y. C. Yu, J. T. W. Wang, C. S. Chang, and L. J. Li, Synthesis of large-area MoS2 atomic layers with chemical vapor deposition, Adv. Mater. **24**, 2320 (2012).
[14] A. Gurarslan, Y. Yu, L. Su, Y. Yu, F. Suarez, S. Yao, Y. Zhu, M. Ozturk, Y. Zhang, and L. Cao, Surface-energy-assisted perfect transfer of centimeter-scale monolayer and few-layer MoS2 films onto arbitrary substrates, ACS Nano **8**, 11522 (2014).
[15] W. W. Cai, A. L. Moore, Y. W. Zhu, X. S. Li, S. S. Chen, L. Shi, and R. S. Ruoff, Thermal Transport in Suspended and Supported Monolayer Graphene Grown by Chemical Vapor Deposition, Nano Lett. **10**, 1645 (2010).
[16] J. Judek, A. P. Gertych, M. Swiniarski, A. Lapinska, A. Duzynska, and M. Zdrojek, High accuracy determination of the thermal properties of supported 2D materials, Sci. Rep. **5** (2015).
[17] H. Malekpour and A. A. Balandin, Raman-based technique for measuring thermal conductivity of graphene and related materials, J. Raman Spectrosc. **49**, 106 (2018).
[18] Y. Yu, Y. Yu, Y. Cai, W. Li, A. Gurarslan, H. Peelaers, D. E. Aspnes, C. G. V. d. Walle, N. V. Nguyen, Y.-W. Zhang, and L. Cao, Exciton-dominated Dielectric Function of Atomically Thin MoS2 Films, Sci. Rep. **5**, 16996 (2015).
[19] Y. Yu, Y. Yu, L. Huang, H. Peng, L. Xiong, and L. Cao, Giant gating tunability of optical refractive index in transition metal dichalcogenide monolayers, Nano Lett. **17**, 3613 (2017).
[20] Y. Li, A. Chernikov, X. Zhang, A. Rigosi, H. M. Hill, A. M. van der Zande, D. A. Chenet, E.-M. Shih, J. Hone, and T. F. Heinz, Measurement of the optical dielectric function of monolayer transition-metal dichalcogenides: MoS 2, Mo S e 2, WS 2, and WS e 2, Phys. Rev. B **90**, 205422 (2014).
[21] E. Yalon, O. z. r. B. Aslan, K. K. Smithe, C. J. McClellan, S. V. Suryavanshi, F. Xiong, A. Sood, C. M. Neumann, X. Xu, and K. E. Goodson, Temperature-dependent thermal boundary conductance of monolayer MoS2 by Raman thermometry, ACS Appl. Mater. Interfaces **9**, 43013 (2017).
[22] S. Lepri, R. Livi, and A. Politi, Studies of thermal conductivity in Fermi–Pasta–Ulam-like lattices, Chaos: An Interdisciplinary, J. Nonlinear Sci. **15**, 015118 (2005).
[23] L. Wang, B. Hu, and B. Li, Logarithmic divergent thermal conductivity in two-dimensional nonlinear lattices, Phys. Rev. E **86**, 040101 (2012).
[24] L. Wang, N. Li, and P. Hänggi, in *Thermal Transport in Low Dimensions* (Springer, 2016), pp. 239.
[25] D. Xiong, J. Wang, Y. Zhang, and H. Zhao, Heat conduction in two-dimensional disk models, Phys. Rev. E **82**, 030101 (2010).
[26] L. Yang, P. Grassberger, and B. Hu, Dimensional crossover of heat conduction in low dimensions, Phys. Rev. E **74**, 062101 (2006).

[27] X. Gu and R. Yang, Phonon transport in single-layer transition metal dichalcogenides: A first-principles study, Appl. Phys. Lett. **105**, 131903 (2014).
[28] K. Xu, A. J. Gabourie, A. Hashemi, Z. Fan, N. Wei, A. B. Farimani, H.-P. Komsa, A. V. Krasheninnikov, E. Pop, and T. Ala-Nissila, Thermal transport in MoS 2 from molecular dynamics using different empirical potentials, Phys. Rev. B **99**, 054303 (2019).
[29] M.-H. Bae, Z. Li, Z. Aksamija, P. N. Martin, F. Xiong, Z.-Y. Ong, I. Knezevic, and E. Pop, Ballistic to diffusive crossover of heat flow in graphene ribbons, Nat. commun. **4**, 1734 (2013).
[30] X. Xu, L. F. Pereira, Y. Wang, J. Wu, K. Zhang, X. Zhao, S. Bae, C. T. Bui, R. Xie, and J. T. Thong, Length-dependent thermal conductivity in suspended single-layer graphene, Nat. commun. **5**, 3689 (2014).
[31] Y. Cai, J. Lan, G. Zhang, and Y.-W. Zhang, Lattice vibrational modes and phonon thermal conductivity of monolayer MoS 2, Phys. Rev. B **89**, 035438 (2014).
[32] H.-Y. Cao, Z.-X. Guo, H. Xiang, and X.-G. Gong, Layer and size dependence of thermal conductivity in multilayer graphene nanoribbons, Phys. Lett. A **376**, 525 (2012).
[33] Y. F. Yu, Y. L. Yu, C. Xu, Y. Q. Cai, L. Q. Su, Y. Zhang, Y. W. Zhang, K. Gundogdu, and L. Y. Cao, Engineering Substrate Interactions for High Luminescence Efficiency of Transition-Metal Dichalcogenide Monolayers, Adv. Func. Mater. **26**, 4733 (2016).
[34] L. Lindsay and D. Broido, Theory of thermal transport in multilayer hexagonal boron nitride and nanotubes, Phys. Rev. B **85**, 035436 (2012).
[35] B. Peng, H. Zhang, H. Shao, Y. Xu, X. Zhang, and H. Zhu, Thermal conductivity of monolayer MoS 2, MoSe 2, and WS 2: interplay of mass effect, interatomic bonding and anharmonicity, RSC Adv. **6**, 5767 (2016).
[36] J. Liu, G.-M. Choi, and D. G. Cahill, Measurement of the anisotropic thermal conductivity of molybdenum disulfide by the time-resolved magneto-optic Kerr effect, J. Appl. Phys. **116**, 233107 (2014).
[37] K. F. Mak, C. H. Lui, and T. F. Heinz, Measurement of the thermal conductance of the graphene/SiO 2 interface, Appl. Phys. Lett. **97**, 221904 (2010).
[38] R. Prasher, Acoustic mismatch model for thermal contact resistance of van der Waals contacts, Appl. Phys. Lett. **94** (2009).
[39] E. T. Swartz and R. O. Pohl, Thermal-Boundary Resistance, Rev. Mod. Phys.**61**, 605 (1989).
[40] H. B. Zhou and G. Zhang, General theories and features of interfacial thermal transport, Chin.Phys. B **27** (2018).
[41] X. Liu, G. Zhang, and Y.-W. Zhang, Thermal conduction across the one-dimensional interface between a MoS 2 monolayer and metal electrode, Nano Res. **9**, 2372 (2016).
[42] J. Kimling, A. Philippi-Kobs, J. Jacobsohn, H. P. Oepen, and D. G. Cahill, Thermal conductance of interfaces with amorphous SiO2 measured by time-resolved magneto-optic Kerr-effect thermometry, Phys. Rev. B **95** (2017).
[43] C. J. Glassbrenner and G. A. Slack, Thermal Conductivity of Silicon + Germanium from 3 Degrees K to Melting Point, Phys. Rev. **134**, 1058 (1964).
[44] A. S. Grove, *Physics and Technology of Semiconductor Devices* (Wiley New York, 1967).
[45] E. Yalon, O. B. Aslan, K. K. H. Smithe, C. J. McClellan, S. V. Suryavanshi, F. Xiong, A. Sood, C. M. Neumann, X. Q. Xu, K. E. Goodson, T. F. Heinz, and E. Pop, Temperature-Dependent Thermal Boundary Conductance of Monolayer MoS2 by Raman Thermometry, ACS Appl. Mater. Interfaces **9**, 43013 (2017).
[46] E. Yalon, C. J. McClellan, K. K. H. Smithe, M. M. Rojo, R. L. Xu, S. V. Suryavanshi, A. J. Gabourie, C. M. Neumann, F. Xiong, A. B. Farimani, and E. Pop, Energy Dissipation in Monolayer MoS2 Electronics, Nano Lett. **17**, 3429 (2017).

[47] P. Yasaei, C. J. Foss, K. Karis, A. Behranginia, A. I. El-Ghandour, A. Fathizadeh, J. Olivares, A. K. Majee, C. D. Foster, F. Khalili-Araghi, Z. Aksamija, and A. Salehi-Khojin, Interfacial Thermal Transport in Monolayer MoS2- and Graphene-Based Devices, Adv. Mater. Interfaces **4** (2017).
[48] A. Aiyiti, X. Bai, J. Wu, X. Xu, and B. Li, Measuring the thermal conductivity and interfacial thermal resistance of suspended MoS2 using electron beam self-heating technique, Sci. Bull. **63**, 452 (2018).
[49] X. Gu, Y. Wei, X. Yin, B. Li, and R. Yang, Colloquium: Phononic thermal properties of two-dimensional materials, Rev. Mod. Phys. **90**, 041002 (2018).
[50] I. Jo, M. T. Pettes, E. Ou, W. Wu, and L. Shi, Basal-plane thermal conductivity of few-layer molybdenum disulfide, Appl. Phys. Lett. **104**, 201902 (2014).
[51] N. Peimyoo, J. Shang, W. Yang, Y. Wang, C. Cong, and T. Yu, Thermal conductivity determination of suspended mono-and bilayer WS 2 by Raman spectroscopy, Nano Res. **8**, 1210 (2015).
[52] S. Sahoo, A. P. Gaur, M. Ahmadi, M. J.-F. Guinel, and R. S. Katiyar, Temperature-dependent Raman studies and thermal conductivity of few-layer MoS2, The J. Phys. Chem. C **117**, 9042 (2013).
[53] Y. Hong, L. Li, X. C. Zeng, and J. Zhang, Tuning thermal contact conductance at graphene–copper interface via surface nanoengineering, Nanoscale **7**, 6286 (2015).
[54] Y. K. Koh, M.-H. Bae, D. G. Cahill, and E. Pop, Heat conduction across monolayer and few-layer graphenes, Nano Lett.**10**, 4363 (2010).
[55] Z. Chen, W. Jang, W. Bao, C. Lau, and C. Dames, Thermal contact resistance between graphene and silicon dioxide, Appl. Phys. Lett. **95**, 161910 (2009).
[56] See Supplemental Material at [URL will be inserted by publisher] for more data on the Raman photothermometry measurement and tabulated experimental data.